

A Stabilization Mechanism of Zirconia Based on Oxygen Vacancies Only*

Stefano Fabris,[†] Anthony T. Paxton and Michael W. Finnis

*Atomistic Simulation Group, Department of Pure and Applied Physics, Queen's University,
Belfast BT7 1NN, United Kingdom*

(September 15, 2018)

Abstract

The microscopic mechanism leading to stabilization of cubic and tetragonal forms of zirconia (ZrO_2) is analyzed by means of a self-consistent tight-binding model. Using this model, energies and structures of zirconia containing different vacancy concentrations are calculated, equivalent in concentration to the charge compensating vacancies associated with dissolved yttria (Y_2O_3) in the tetragonal and cubic phase fields (3.2 and 14.4% mol respectively). The model is shown to predict the large relaxations around an oxygen vacancy, and the clustering of vacancies along the $\langle 111 \rangle$ directions, in good agreement with experiments and first principles calculations. The vacancies alone are shown to explain the stabilization of cubic zirconia, and the mechanism is analyzed.

I. INTRODUCTION

Stabilized zirconias are materials of outstanding technological importance¹. Pure zirconia (ZrO_2) is monoclinic (m) at zero temperature (space group $P2_1/c$, Ref. 2,3); upon increase of the temperature (at zero pressure) the material transforms to tetragonal (t) and then to a cubic (c) fluorite structure (space groups $P4_2/nmc$ and $Fm3m$, respectively).^{4–7} These phase transitions induce large volume changes and make the pure material unsuitable for applications. The addition of lower-valence oxides like CaO , MgO , or Y_2O_3 disfavour the m phase, stabilizing more symmetric structures with cubic and tetragonal symmetry.⁸ On increasing dopant concentration, the material transforms to a tetragonal (t^*) form, called partially stabilized, and then to a cubic (c^*) one, called fully stabilized. The amount of

*Supported by the European Science Foundation, by the EPSRC for funding under Grants No. L66908 and No. L08380, and by the European Communities HCM Network “Electronic Structure Calculations of Materials Properties and Processes for Industry and Basic Science” under grant No. ERBFMRXCT980178

[†]Present address: Max-Planck-Institut für Metallforschung, Heisenbergstr. 3, D-70569 Stuttgart, Germany.

doping needed for stabilization is quite substantial (no less than 8 % mol Y_2O_3 to achieve full stabilization^{9–11}), and the electrostatic neutrality of this rather ionic material is maintained by oxygen vacancies. In this case one vacancy is required for every two yttrium ions.

The simultaneous presence of dopant cations and oxygen vacancies in large concentration means that the local atomic environments in the stabilized material are very different from the corresponding stoichiometric (t and c) phases. Despite the analogy in the sequences $m-t-c$ and $m-t^*-c^*$, there is no clear picture of the microscopic mechanisms of stabilization to parallel our understanding of the pure material: the most relevant issue concerns the respective roles of impurity cations and of oxygen vacancies¹².

We address this issue by means of a self-consistent tight-binding model, which was parameterized on the electronic and structural properties of pure zirconia^{13,14}. The method was used to calculate the temperature evolution of the free energy surfaces governing the $c-t$ phase transition, which was then described within the Landau theory of phase transformations¹⁵. These results are the starting point for the present approach to the stabilization mechanism, which is based on the qualitative analogy between isothermal and isoconcentration lines in the high-temperature region of the $\text{ZrO}_2\text{-Y}_2\text{O}_3$ phase-diagram. At fixed concentration, higher temperatures destabilize the tetragonal phases t and t^* , favouring the cubic ones c and c^* . Similarly, at fixed temperature, higher amount of impurities stabilize the cubic phases.

The position of the oxygen vacancy which is associated with each pair of Y atoms has been a subject of some discussion. Even though there are experimental data supporting the case in which Y is nearest neighbor (NN) to the vacancy^{16–18}, the most recent experiments^{19–27,11} suggest that Y is next nearest neighbor (NNN) to the vacancy. First-principles calculations^{28,29} agree with the latter result, showing that the Y NNN position is energetically favoured by 0.34 eV with respect to the NN position.²⁸ The analysis of Li and coworkers^{22–27} suggests that the Y atoms have a composition-independent 8 fold coordination shell (like in the perfect fluorite structure c) in both the c^* and t^* lattice types, further supporting the hypothesis that the dopants are on average NNN to the vacancies. The presence of oxygen vacancies, together with the Y in the NNN position, reduces the average coordination number of the zirconium atoms from 8, as in the c structure, to values closer to 7, similar to the m phase. Besides the fact that the Y atoms are 8-fold coordinated in both the stabilized structures, on the basis of the K edge in x-ray-absorption spectra, Li and coworkers^{22–27} conclude that the perturbation in the neighborhood of the dopant cations is small and short-ranged.

From these considerations, it is tempting to propose a physical picture in which the dopant cations, located in fluorite-like cation lattice sites NNN to the vacancies, do not take an active part in the stabilization mechanism, which is dominated by the crystal distortions around the oxygen vacancies. We now investigate the consequences of this hypothesis, by neglecting altogether the presence of the dopant atoms, therefore isolating the role played by oxygen vacancies in the stabilization of the c^* and t^* forms of zirconia.

In Section II, the model is shown to reproduce the local atomic and electronic structure around an isolated oxygen vacancy predicted by first-principles calculations. The atomistic structures resulting from modelling partially and fully stabilized zirconia are then presented in Section III, and the results are discussed in Section IV. Final remarks and a summary are made in Section V.

II. THE ISOLATED VACANCY: STRUCTURAL AND ELECTRONIC PROPERTIES

As a preliminary step towards the modelling of stabilized zirconia, the structural and electronic properties of a model crystal structure containing an isolated oxygen vacancy are first addressed. The same system was studied from first principles by Stapper and coworkers:²⁸ a cubic 96-sites super-cell of 95 atoms in the fluorite structure containing one vacant oxygen lattice site, that we define as V_1 . The vacancy is in the +2 charge state (one O^{2-} ion missing). In the real material, the charge of the $V_O^{\bullet\bullet}$ defect is compensated by the dopant substitutional cations Y'_{Zr} . In our analysis, we mimic the presence of the charge-compensating Y atoms by distributing their charge over the 32 Zr cations, so that the cell is electrostatically neutral. The electronic structure in the neighborhood of the vacancy is described by the dangling orbitals of its neighbouring atoms.

We define as *unrelaxed* the configuration in which all the atoms are in the centrosymmetric fluorite positions, and as *relaxed* the crystal structure resulting from the static optimization of the atomic coordinates.

As the crystal is allowed to relax the Zr atoms NN to the vacancy radially shift outward along $\langle 111 \rangle$ directions, and the first shell of anions around the vacancy (NN O atoms) contract inward along $\langle 100 \rangle$ directions. This relaxation pattern is driven by the electrostatics and is shown in Figure 1. The atomic displacements predicted by the SC-TB are compared to the first-principles results²⁸ in Table I. It may be noticed how the first-principles structural relaxations are well reproduced by the SC-TB model, *without* the inclusion of extra adjustable parameters.

Figure 2 shows the total density of states (DOS) calculated with the SC-TB model for both the relaxed and unrelaxed configurations. The DOS are plotted with respect to the energy of the highest occupied level. Because of the choice of the reference energy, the valence $2p$ oxygen bands have negative energies. Above the bandgap, it is possible to identify the crystal field splitting of the zirconium d bands. In the undistorted case (left panel), the arrow points to a sharp peak within the bandgap, also predicted by other calculations.^{30,31} The corresponding partial DOS shows that this peak corresponds to the NN Zr d bands with symmetry E . The atomic relaxation (right panel) shifts the isolated peak back into the conduction band, as predicted by first principles calculations.²⁸

These results of the SC-TB model may be interpreted by considering the perturbation in the periodic electrostatic (Madelung) potential in the stoichiometric c structure caused by the presence of an oxygen vacancy $V_O^{\bullet\bullet}$. This defect increases the Madelung potential on the neighbouring sites, thereby lowering the energy of the d states of the Zr ions NN to the vacancy with respect to the d states of the bulk Zr ions far from the defect. This perturbation in the Madelung potential at the nearest neighbour Zr sites is responsible for the isolated peak in the bandgap of the unrelaxed defective structure, marked by the arrow in Figure 2. The atomic relaxation effectively restores the homogeneity of the Madelung potential in the neighbourhood of the vacancy, pushing the NN Zr d levels back upwards.

III. STABILISED ZIRCONIA: STRUCTURAL STABILITY

The study of the stabilization mechanism is based on static and dynamic simulations of two 96-site super-cells which were chosen as representative systems. The first one, denoted as V_1 , contains one vacancy. This system corresponds to 3.2% mol Y_2O_3 and therefore it should be in the field of stability of the t^* phase. Similarly, the second super-cell V_4 contains 4 vacancies and corresponds to 14.4% mol Y_2O_3 , which is in the phase-field of fully stabilized zirconia c^* . The electrostatic neutrality of the super-cells was ensured by distributing the compensating ionic charge of the dopant atoms over the 32 Zr cations. For each system, two separate sets of calculations were carried out: static relaxations and molecular dynamics (MD). The dynamics of the systems were simulated for 25 ps with a time-step of 5 fs, constraining the temperature at 300 K with a Nosè-Hoover thermostat^{32–34}.

A. Partially stabilized zirconia

The static minimization of the V_1 super-cell has already been described. Further analysis of the structure reveals that the atomic configuration obtained in Section II is metastable, corresponding to a saddle point in the potential energy. By perturbing the relaxed configuration obtained in Section II, a secondary structural modification further lowers the total energy of the cell, similar to the tetragonal distortion of the oxygen sublattice in pure stoichiometric c zirconia (soft X_2^- mode of vibration).

According to the energy surface governing the $c-t$ relationship,¹⁵ the internal tetragonal distortion of the oxygen sublattice drives the external tetragonal distortion of the unit-cell. As a consequence, the relaxed configuration is expected to be further minimized by a non unitary c/a ratio. Indeed, allowing the tetragonality of the cell to adjust, the minimum energy is obtained for $c/a = 1.02$. The corresponding equilibrium structure is shown in Figure 3. The anions and cations are represented with light and dark circles respectively and the arrows point to the oxygen column containing the vacancy, which is behind the first visible oxygen ion. The projection on the $x-y$ plane (left) shows the same pattern obtained with the static minimization. The NN cations move away from the vacancy and the NN anions contract inward. The right panel shows the projection along the $x-z$ plane: the tetragonal distortion of the oxygen sublattice is very clear. Note the perturbation in the neighborhood of the vacancy arising from the superposition of the tetragonal distortion and the vacancy-induced radial displacement field.

The MD simulation of the V_1 super-cell shows that this atomic structure is stable and does not undergo any further structural modification. The atomic configuration obtained by averaging the atomic positions over the last 20 ps coincide with the one obtained with the static minimization, shown in Figure 3.

The similarity between the t^* and t structures is also evident from the Radial Distribution Function (RDF) shown in Figure 4. In agreement with the experimental measurements^{16,17,22–27}, the splitting of the first peak in the Zr-O RDF, a sign of the oxygen sublattice being tetragonally distorted, is also present in the RDF of the t^* phase. The first peak in the O-O RDF is exactly the same in both the tetragonal phases, while the disorder introduced by the vacancy slightly modifies the second O-O coordination shell. The Zr-Zr

RDF indicates that the cation sublattice is nearly *fcc*. Arrows in Figure 4 indicate the available experimental values for 3% and 15% mol Y_2O_3 ^{22–27}.

B. Fully stabilised zirconia

The c^* phase was modelled by distributing four vacancies in the super-cell. Here we consider two possible high-symmetry vacancy configurations. In the first one, the vacancies were distributed in the cell by maximizing the defect-defect separation, by setting the four vacancies on a *fcc* lattice, with a defect-defect distance of $\sqrt{2}a_0$ ($a_0=9.61$ a.u.= 5.09 Å is the lattice constant of the cubic structure). In the second configuration, the four vacancies were aligned along the $\langle 111 \rangle$ direction, with a defect-defect minimum distance of $\sqrt{3}/2 a_0$. The SC-TB model shows that the second configuration is more stable than the first one by 0.1 Ry per super-cell. It therefore predicts the clustering of vacancies along the $\langle 111 \rangle$ direction, as observed experimentally^{11,35,36} and from first-principles calculations.²⁹ The results for the most stable of the two vacancy configurations, which we refer to as the V_4 super-cell, are described in what follows.

The static relaxation was started with all the atoms in the fluoritic centro-symmetric positions. In this case, only one structural modification was observed. The system evolved towards the atomic configuration shown in Figure 5. The local distortions around the vacancies lock the c^* crystal in a distorted configuration, suppressing the tetragonal distortion of the oxygen sublattice. The same structure was then obtained by MD simulation of the V_4 super-cell. The local atomic environment is very different from that of the fluorite structure: 14 cations out of 32 are 7 fold coordinated and the majority of the oxygen ions are not in centro-symmetric positions. The minimum energy is obtained for a perfect cubic super-cell ($c/a = 1$).

Despite these distortions, the RDF shown in Figure 4 suggests that the structure of the V_4 is, on average, cubic. The first peak of the Zr-O component confirms that the oxygen sublattice is not tetragonally distorted. The calculated average Zr-O distance compares very well with the experimental one in 15% mol yttria stabilized zirconia^{22–27}, shown by the arrow. In the tetragonal structures, the O-O second coordination shell shows a characteristic three-peaked RDF. The corresponding RDF of the c^* phase, shows only a single peak centered at $r = a_0 \sqrt{2} = 6.8$ a.u., which is the second shell O-O distance in the perfect cubic lattice. Because of the outward displacement of the large number of Zr atoms NN to the vacancies, the first Zr-Zr peak is shifted to smaller r , which is also experimentally observed (see arrow in Figure 4c). Apart from this detail, the Zr-Zr RDF shows complete similarity with the other cases and therefore the Zr sublattice is *fcc*, even in the V_4 supercell.

IV. DISCUSSION

Our results corroborate some of the early experimental observations on stabilized zirconia and on other compounds with the general formula M_7O_{12} .^{35,36} These reported a strong distortion of the oxygen sublattice, with the NN O atoms relaxing towards the vacancy by ≈ 0.3 Å and the NN Zr relaxing away from the vacancy by less than 0.2 Å.³⁵ Moreover, in the special case of the $\text{Zr}_3\text{M}_4\text{O}_{12}$ compounds, the difference between the ordered and

disordered fluorite structures was determined by the arrangement of the oxygen vacancies,³⁵ which were reported to lie along the $[111]$ directions.³⁶

When the results described in the previous Sections are considered in the context of the $c \leftrightarrow t$ phase transition in pure zirconia,¹⁴ they also provide insight on how the structural distortions around the oxygen vacancies affect the relative stability of the tetragonal and cubic phases. The relationship between the c and t forms is governed by a temperature-dependent double-well in the potential energy. At low temperature, the cubic phase c is structurally unstable and it lowers the energy by distorting the oxygen sublattice along the X_2^- mode of vibration. The extent of this distortion is measured by the order parameter δ . The 0 K double-well for the $c - t$ structures is shown in Figure 6 by a solid line labelled t .

The static relaxations showed that both the unrelaxed cells V_1 and V_4 are unstable with respect to the short-range isotropic relaxation around the vacancies. Moreover, our atomistic simulations suggest that the V_1 cell is also unstable with respect to the tetragonal distortion. Let us now simply superimpose these two displacement fields to see how the oxygen vacancies, considered as centers of dilations, modifies the energy double-well. In the following, the statically relaxed configurations of V_1 and V_4 which show the radial displacements only, are taken as reference systems, to which we apply the tetragonal distortion δ . The results are shown in Figure 6.

Similarly to the c structure, the defective V_1 cell is unstable with respect to the tetragonal distortion: the atomic relaxations around the vacancy partially reduce the height and width of the double well (Figure 6). A static minimization from the minimum of the double-well leads to the same structure obtained by averaging over the MD configurations (Figure 3), and showing that the finite-temperature equilibrium configuration is not just a superposition of the two displacement fields.

On the other hand, the reference V_4 cell is stable with respect to the tetragonal distortion of the oxygen sublattice and there is no double-well in the total energy (Figure 6). The energy profile is highly anharmonic, just as the high-temperature one in the free-energy for the pure phase¹⁴. This means that in our model for c^* , it is possible to shift entire column of oxygen atoms by 5-10 % of the Zr-O interatomic distance at no energy cost, with important implications for the mobility of defects and therefore for transport phenomena in stabilized zirconia. We know from our previous simulations, and it is not surprising, that in a flat well of this form the average structure at finite temperature is cubic.

V. CONCLUSIONS

In conclusion, partially and fully stabilized zirconia were modelled by introducing respectively one and four vacancies in 96-site cubic super-cell (V_1 and V_4 , respectively). Energetics and atomic structures of the defective super-cells were calculated with a SC-TB model which was parameterized on the properties of pure stoichiometric zirconia.

The analysis of the V_1 and V_4 equilibrium crystal structures suggests a possible explanation of the stabilization mechanism. When the concentration of vacancies is low, as in the V_1 super-cell, a relatively large volume of crystal is left in the fluorite structure, and it undergoes the tetragonal distortion just as the stoichiometric material in the c -phase would. Because this distortion involves the coordinated motion of all the oxygens, also the

atoms neighboring the defects are dragged along the tetragonal distortion of the oxygen sublattice (see Figure 3).

When the concentration of defects is high, as in the V_4 super-cell, there is virtually no undistorted cubic region in the statically relaxed super-cell; every oxygen atom is either itself a neighbor of a vacant site, or at least four of its six neighboring oxygen atoms are. Thus there is virtually no region in which the local atomic environment is close to fluorite, which could undergo the tetragonal distortion (see Figure 5), and the radial distortions around the vacancies dominate the finite-temperature equilibrium configuration. The resulting atomic structure is cubic only by averaging over relatively large number of atoms (≈ 100), but the short-range atomic structure does not have cubic symmetry.

These results show that the stabilization of the t^* and c^* structures may be achieved in theory by doping zirconia crystals with oxygen vacancies only, and support the idea that the electronic and structural properties of stabilized zirconia are controlled by the structural disorder around the oxygen vacancies, rather than by the substitutional dopant cations.

REFERENCES

- ¹ "Science and Technology of Zirconia", in *Advances in Ceramics*, Vol. 3. Edited by A. H. Heuer and L. W. Hobbs. The American Ceramic Society, Columbus, Ohio, 1981).
- ² J. D. McCullough and K. N. Trueblood, "The Crystal Structure of Baddeleyite," *Acta Crystallogr.*, **12** 507-11 (1959).
- ³ D. K. Smith and H. W. Newkirk, "The Crystal Structure of Baddeleyite and its Relation to the Polymorphism of ZrO_2 ", *Acta Crystallogr.*, **18** 983-91 (1965).
- ⁴ C. J. Howard, R. J. Hill, and B. E. Reichert, "Structures of the ZrO_2 Polymorphs at Room Temperature by High-Resolution Neutron Powder Diffraction," *Acta Crystallogr.*, **B44** 116-20 (1988).
- ⁵ G. Teufer, "The Crystal Structure of Tetragonal ZrO_2 ," *Acta Crystallogr.*, **15** 1187 (1962).
- ⁶ P. Aldebert and J. P. Traverse, "Structure and Ionic Mobility of Zirconia at High Temperature," *J. Am. Ceram. Soc.*, **68** [1] 34 (1985).
- ⁷ R. J. Ackermann, S. P. Garg, and E. G. Rauh, "High-temperature phase diagram for the system Zr-O ," *J. Am. Ceram. Soc.*, **60** [7-8] 341-5 (1977).
- ⁸ E. C. Subbarao, "Zirconia-an overview"; pp. 1-24 in "Science and Technology of Zirconia", *Advances in Ceramics*, Vol. 3. Edited by A. H. Heuer and L. W. Hobbs. The American Ceramic Society, Columbus, Ohio, 1981)
- ⁹ C. F. Grain, "Phase Relations in the ZrO_2 - MgO system," *J. Am. Ceram. Soc.*, **50** [6] 288 (1967).
- ¹⁰ V. S. Stubican and S. P. Ray, "Phase Equilibria and Ordering in the System ZrO_2 - CaO ," *J. Am. Ceram. Soc.*, **60** [11-12] 534-7 (1977).
- ¹¹ J. P. Goff, W. Hayes, S. Hull, M. T. Hutchings, and K. N. Clausen, "Defect Structure of Ytria-stabilised Zirconia and its Influence on the Ionic Conductivity at Elevated Temperatures," *Phys. Rev. B*, **59** [22] 14202-19 (1999).
- ¹² E. V. Stefanovich, A. L. Shluger, and C. R. A. Catlow, "Theoretical Study of the Stabilization of the Cubic-phase ZrO_2 by Impurities," *Phys. Rev. B*, **49** [17] 11560-71 (1994).
- ¹³ M. W. Finnis, A. T. Paxton, M. Methfessel, and M. van Schilfgaarde, "Crystal Structures of Zirconia from First Principles and Self-consistent Tight-binding," *Phys. Rev. Lett.*, **81** [23] 5149-52 (1998).
- ¹⁴ S. Fabris, A. T. Paxton, and M. W. Finnis, "Relative Energetics and Structural Properties of Zirconia using a Self-consistent Tight-binding Model," *Phys. Rev. B*, **61** [10] 6617-30 (2000).
- ¹⁵ S. Fabris, A. T. Paxton, and M. W. Finnis, "Free Energy and Molecular Dynamics Calculations for the Cubic-tetragonal Phase Transition in Zirconia," *Phys. Rev. B*, **63** [9] 094101-13 (2001).
- ¹⁶ M. H. Tuilier, J. Dexpert-Ghys, H. Dexpert, and P. Lagarde, "X-ray Absorption Study of the ZrO_2 - Y_2O_3 System," *J. Solid State Chem.*, **69** [1] 153-61 (1987).
- ¹⁷ H. Morikawa, Y. Shimizugawa, F. Murumo, T. Harashawa, H. Ikawa, K. Tohji, and Y. Udagawa, "Local Structures around Y Atoms in Y_2O_3 -stabilized Tetragonal ZrO_2 ," *J. Jpn. Ceram. Soc.*, **96** [3] 253-8 (1988).
- ¹⁸ D. Steele and B. E. F. Fender, "The Structure of Cubic ZrO_2 : $\text{YO}_{1.5}$ Solid Solutions by Neutron Scattering," *J. Phys. C.: Solid State Phys.*, **7** [1] 1-11 (1974).

- ¹⁹ C. R. A. Catlow, A. V. Chadwick, G. N. Greaves, and L. M. Moroney, "EXAFS Study of Yttria-stabilized Zirconia," *J. Am. Ceram. Soc.*, **69** [3] 272-7 (1986).
- ²⁰ B. W. Veal, A. G. Mckale, A. P. Paulikas, S. J. Rothman, and L. J. Nowicki, "EXAFS Study of Yttria Stabilized Cubic Zirconia," *Physica B*, **150** [1-2] 234-40 (1988).
- ²¹ D. Komyoji, A. Yoshiasa, T. Moriaga, S. Emura, F. Kanamaru, and K. Koto, "EXAFS Study of the Fluorite-type Compounds in the Systems (1-x)ZrO₂-(2-x)YO_{1.5} (x=0.18)," *Solid State Ion.*, **50** [3-4] 291-301 (1992).
- ²² P. Li, I. Chen, and J. E. Penner-Hahn, "X-ray-absorption Studies of Zirconia Polymorphs. I. Characteristic Local Structures," *Phys. Rev. B*, **48** [14] 10063-73 (1993).
- ²³ P. Li, I. Chen, and J. E. Penner-Hahn, "X-ray-absorption Studies of Zirconia Polymorphs. II. Effect of Y₂O₃ Dopant on ZrO₂ Structure," *Phys. Rev. B*, **48** [14] 10074-81 (1993).
- ²⁴ P. Li, I. Chen, and J. E. Penner-Hahn, "X-ray-absorption Studies of Zirconia Polymorphs. III. Static Distortion and Thermal Distortion," *Phys. Rev. B*, **48** [14] 10082-89 (1993).
- ²⁵ P. Li, I. Chen, and J. E. Penner-Hahn, "Effect of Dopants on Zirconia Stabilization—An X-ray Absorbption Study: I, Trivalent Dopants," *J. Am. Ceram. Soc.*, **77**, 118-28 (1994).
- ²⁶ P. Li, I. Chen, and J. E. Penner-Hahn, "Effect of Dopants on Zirconia Stabilization—An X-ray Absorbption Study: II, Tetravalent Dopants," *J. Am. Ceram. Soc.*, **77**, 1281-88 (1994).
- ²⁷ P. Li, I. Chen, and J. E. Penner-Hahn, "Effect of Dopants on Zirconia Stabilization—An X-ray Absorbption Study: III, Charge-Compensating Dopants," *J. Am. Ceram. Soc.*, **77**, 1289-95 (1994).
- ²⁸ G. Stapper, M. Bernasconi, N. Nicoloso, and M. Parrinello, "Ab-initio Study of Structural and Electronic Properties of Yttria-stabilized Zirconia," *Phys. Rev. B*, **59** [2] 7978-10 (1999).
- ²⁹ A. Bogicevic, C. Wolverton, G. M. Crosbie, and E. B. Stechel, "Defect Ordering in Aliovalently Doped Cubic Zirconia from First Principles," *Phys. Rev. B*, **64** 014106-14 (2001).
- ³⁰ S. E. Kul'kova and O. N. Muryzhnikova, "The Calculation of the Electronic Structure of Zirconium Dioxide in Cubic and Tetragonal Phases," *Physica B*, **192** [3] 284-90 (1993).
- ³¹ G. A. Ol'khovic, I. I. Naumov, and O. I. Velikokhatnyi, "Band Structure of Cubic ZrO₂ Containing Oxygen Vacancies and Calcium Ions," *J. Phys. Condens. Matter*, **7** [7] 1273-82 (1995).
- ³² S. Nosé, "A Unified Formulation of the Constant Temperature Molecular Dynamics Methods," *J. Chem. Phys.*, **81** [1] 511-19 (1984)
- ³³ S. Nosé, "A Molecular Dynamics Method of Simulation in the Canonical Ensemble", *Mol. Phys.*, **52** [2] 255-68 (1984)
- ³⁴ W. G. Hoover, "Canonical Dynamics: Equilibrium Phase-Space Distributions," *Phys. Rev. A* **31** [3] 1695-7 (1985).
- ³⁵ H. J. Rossell, "Crystal Structures of Some Fluorite-Related M₇O₁₂ Compounds, *J. Solid State Chem.*, **19**[2] 103-111 (1976).
- ³⁶ V. S. Stubican, R. C. Hink, and S. P. Ray, "Phase Equilibria and Ordering in the System ZrO₂-Y₂O₃", *J. Am. Ceram. Soc.*, **61**[1-2] 17-21 (1978)

FIGURE CAPTIONS

FIG.1. Crystal relaxation of the atoms neighbouring an isolated vacancy in a fluorite lattice. Key: Zr black, O dark grey, vacancy light grey.

FIG.2. Total density of states for the relaxed and unrelaxed configurations of the V_1 supercell, calculated with the SC-TB. The 0 of energy is the highest occupied electron state. The arrow points to the energy levels of the Zr atoms NN to the vacancy, split from the d bands of the “bulk” Zr atoms.

FIG.3. Equilibrium crystal structure of the V_1 supercell. The arrow point to the oxygen columns containing the vacancy.

FIG.4. Equilibrium crystal structure of the V_4 supercell. The arrows point to the oxygen columns containing the vacancies.

FIG.5. Radial Distribution Function $g(r)$ obtained from the MD simulations at 300 K for three supercells: t -ZrO₂, V_1 and V_4 . Arrows represent the experimental values for t^* - and c^* -ZrO₂ (Ref. 13).

FIG.6. Total energy vs. tetragonal distortion δ of the oxygen sublattice for three 96-site cells: t pure stoichiometric tetragonal structure; t^* partially stabilized zirconia (V_1 super-cell); c^* fully stabilized zirconia (V_4 super-cell).

TABLES

TABLE I. Atomic displacement (in Å) predicted by the SC-TB model compared to ab initio results.¹

		O NN	Zr NN	O NNN	Zr NNN
DFT	Ref. 28	0.24	0.14	0.04	0.04
SC-TB	this work	0.27	0.18	0.03	0.03

¹The displacements are along the directions shown by the arrows in Figure 1. NN and NNN mean Nearest Neighbour and Next Nearest Neighbour to the defect.

FIGURES

FIG. 1. Crystal relaxation of the atoms neighbouring an isolated vacancy in a fluorite lattice. Key: Zr black, O dark grey, vacancy light grey.

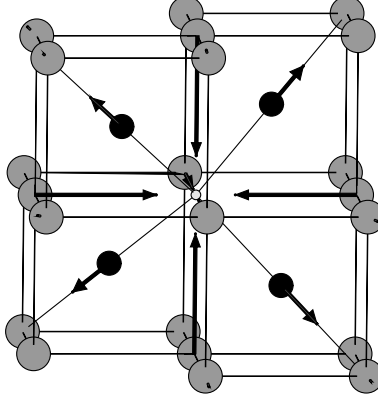


FIG. 2. Total density of states for the relaxed and unrelaxed configurations of the V_1 supercell, calculated with the SC-TB. The 0 of energy is the highest occupied electron state. The arrow points to the energy levels of the Zr atoms NN to the vacancy, split from the d bands of the “bulk” Zr atoms.

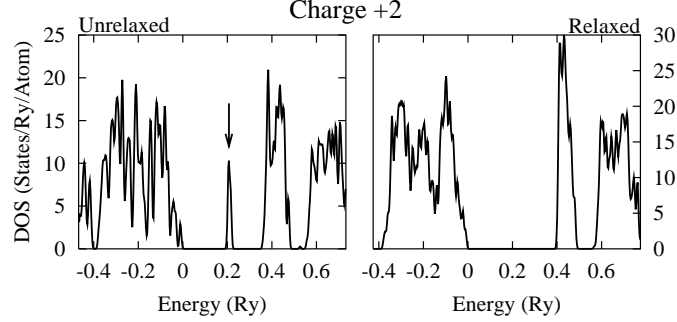


FIG. 3. Equilibrium crystal structure of the V_1 supercell. The arrow point to the oxygen columns containing the vacancy.

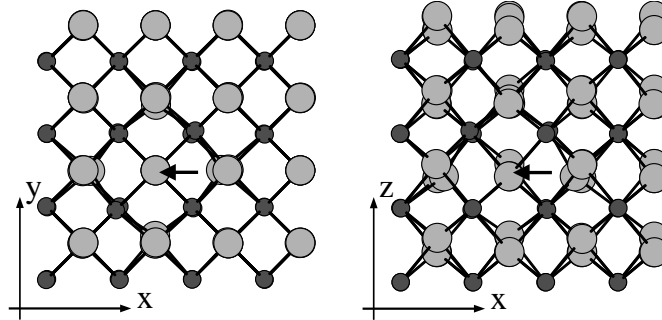


FIG. 4. Radial Distribution Function $g(r)$ obtained from the MD simulations at 300 K for three supercells: t - ZrO_2 , V_1 and V_4 . Arrows represent the experimental values for t^* - and c^* - ZrO_2 (Ref. 13).

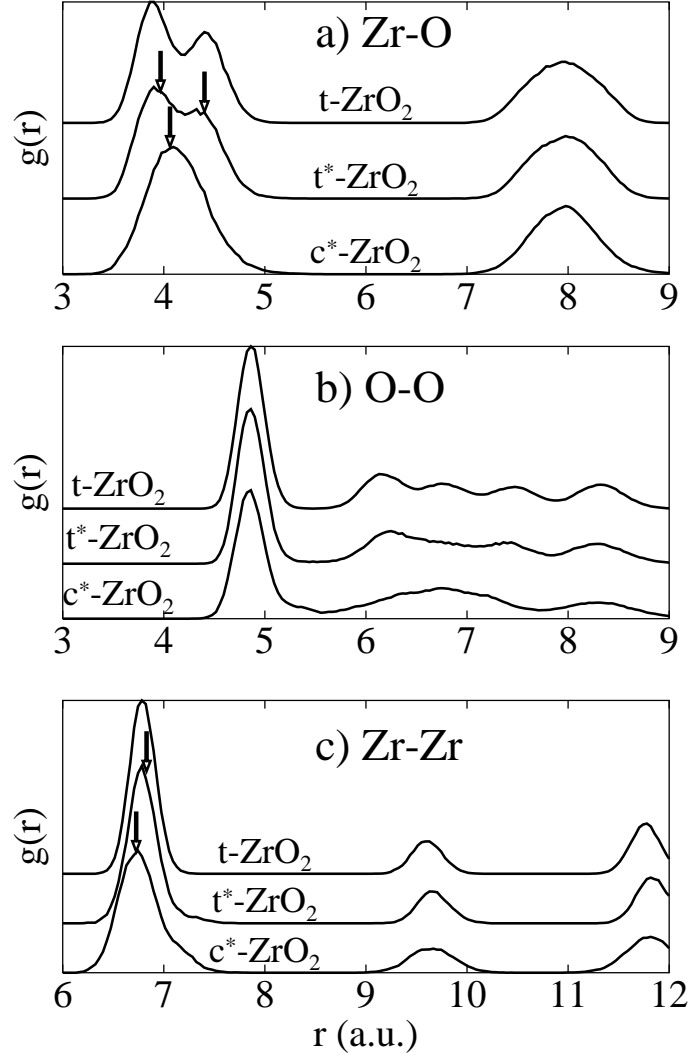


FIG. 5. Equilibrium crystal structure of the V_4 supercell. The arrows point to the oxygen columns containing the vacancies.

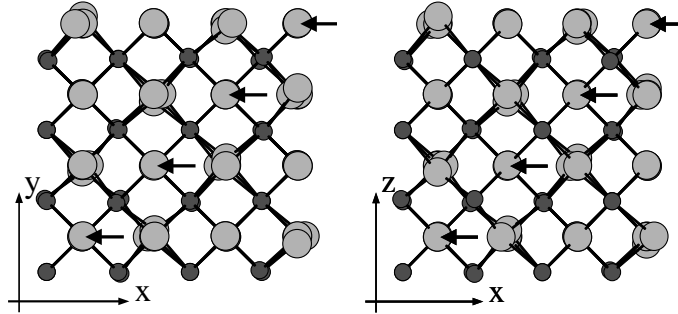


FIG. 6. Total energy vs. tetragonal distortion δ of the oxygen sublattice for three 96-site cells: t pure stoichiometric tetragonal structure; t^* partially stabilized zirconia (V_1 super-cell); c^* fully stabilized zirconia (V_4 super-cell).

